The Receptor-Bound "Empty Pocket" State of the Heterotrimeric G-Protein α-Subunit Is Conformationally Dynamic†

Najmoutin G. Abdulaev,‡ Tony Ngo,§ Eva Ramon,§ Danielle M. Brabazon,|| John P. Marino,*,‡ and Kevin D. Ridge*,§

Center for Advanced Research in Biotechnology, University of Maryland Biotechnology Institute and National Institute of Standards and Technology, Rockville, Maryland 20850, Center for Membrane Biology, Department of Biochemistry and Molecular Biology, University of Texas Health Science Center, Houston, Texas 77030, and Department of Chemistry, Loyola College in Maryland, Baltimore, Maryland 21210

Received May 31, 2006; Revised Manuscript Received August 29, 2006

ABSTRACT: Heterotrimeric G-protein activation by a G-protein-coupled receptor (GPCR) requires the propagation of structural signals from the receptor-interacting surfaces to the guanine nucleotide-binding pocket. To probe conformational changes in the G-protein α-subunit (G_α) associated with activated GPCR (R*) interactions and guanine nucleotide exchange, high-resolution solution NMR methods are being applied in studying signaling of the G-protein, transducin, by light-activated rhodopsin. Using these methods, we recently demonstrated that an isotope-labeled G_α reconstituted heterotrimer forms functional complexes under NMR experimental conditions with light-activated, detergent-solubilized rhodopsin and a soluble mimic of R*, both of which trigger guanine nucleotide exchange [Ridge, K. D., et al. (2006) *J. Biol. Chem. 281*, 7635−7648]. Here, it is shown that both light-activated rhodopsin and the soluble mimic of R* form trapped intermediate complexes with a GDP-released "empty pocket" state of the heterotrimer in the absence of GTP (or GTPγS). In contrast to guanine nucleotide-bound forms of G_α, the NMR spectra of the GDP-released, R*-bound empty pocket state of G_α display severe line broadening suggestive of a dynamic intermediate state. Interestingly, the conformation of a GDP-depleted, Mg^{2+}-bound state of G_α generated in a manner independent of R* does not exhibit a similar degree of line broadening but rather appears structurally similar to the GDP/Mg^{2+}-bound form of the protein. Taken together, these results suggest that R*-mediated changes in the receptor-interacting regions of G_α, and not the absence of bound guanine nucleotide, are the predominant factors which dictate G_α conformation and dynamics in this R*-bound state of the heterotrimer.

Crystallographic studies on various guanine nucleotide-bound states of heterotrimeric G-protein α-subunits (G_α),[1] G-protein βγ-subunits ($G_{\beta\gamma}$), and the intact holoenzyme ($G_{\alpha\beta\gamma}$) have been instrumental in providing high-resolution structural information about this important class of intracellular signaling proteins (*1*−*10*). In combination with numerous biochemical and mutational studies, a molecular understanding of some of the transformations accompanying GDP−GTP exchange and GTP hydrolysis, particularly those in the flexible switch regions of the GTPase domain of G_α, have been revealed. Similarly, the three-dimensional crystal structure of the inactive state of the G-protein-coupled receptor (GPCR) rhodopsin (*11*−*15*) has had a significant impact on our understanding of this visual photoreceptor that, by extension, has also provided keen insights into the structure and function of other members of the rhodopsin-like family (family A) of GPCRs. In particular, the rhodopsin structure has provided a template for assimilating and interpreting much of the accumulated biochemical, mutational, and biophysical data that attempts to understand conformational changes associated with formation of the active signaling state, R* (*16*, *17*). While various models of R*-catalyzed G-protein activation (*18*−*23*) have been developed using available crystal structures and biochemical data, the structural basis for the R*−G-protein interaction remains poorly defined yet will likely be required for the

† This work was supported by NIH Grant EY016493 to K.D.R. and J.P.M., NIH Grant EY013286 and Robert A. Welch Foundation (AU-1613) awards to K.D.R., Research Corporation Grant CC5250 to D.M.B., and a fellowship from the Spanish Ministry of Science to E.R. NMR instrumentation was supported in part by National Institutes of Health/National Center for Research Resources Grant RR015744, the National Institute of Standards and Technology, and the W. M. Keck Foundation.

* To whom correspondence should be addressed. J.P.M.: fax, (240) 314-6255; phone, (240) 314-6160; e-mail, john.marino@nist.gov. K.D.R.: fax, (713) 500-0545; phone, (713) 500-5908; e-mail, kevin.d.ridge@uth.tmc.edu.

‡ University of Maryland Biotechnology Institute and National Institute of Standards and Technology.

§ University of Texas Health Science Center.

|| Loyola College in Maryland.

[1] Abbreviations: G_α, α-subunit of a heterotrimeric G-protein; $G_{\beta\gamma}$, βγ-subunits of a heterotrimeric G-protein; GPCR, G-protein-coupled receptor; R*, agonist-activated form of a GPCR; GTP, guanosine triphosphate; GDP, guanosine diphosphate; G_t, transducin; $G_{t\alpha}$, α-subunit of transducin; $G_{t\beta\gamma}$, βγ-subunits of transducin; GTPγS, guanosine 5′-*O*-3-thiotriphosphate; AlF_4^-, aluminum fluoride; ChiT, prodomain-released chimeric G_α; ROS, rod outer segment; HPTRX−CDEF, protein chimera containing segments from the CD and EF loops of bovine opsin grafted into a thioredoxin loop; 1D, one-dimensional; 2D, two-dimensional; HSQC, heteronuclear single-quantum correlation.

10.1021/bi061088h CCC: $33.50
Published on Web 10/07/2006

Scheme 1: Reaction Pathway for Transducin Activation by Photolyzed Rhodopsin[a]

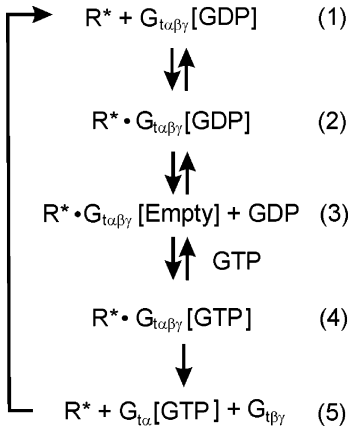

[a] Light-activated rhodopsin (R*) binds to the GDP-bound form of transducin ($G_{t\alpha\beta\gamma}$[GDP]) and induces GDP release to form the nucleotide-free R*·$G_{t\alpha\beta\gamma}$[empty] complex. Uptake of GTP by $G_{t\alpha\beta\gamma}$[empty] leads to the transient formation of the R*·$G_{t\alpha\beta\gamma}$[GTP] complex and subsequent release and dissociation of $G_{t\alpha}$[GTP] and $G_{t\beta\gamma}$ from R*.

molecular mechanisms underlying these initial steps in the signal transfer process to be fully understood.

To probe for conformational changes in the G_α subunit accompanying signal propagation from R* to the G-protein, we are using high-resolution NMR methods to study the interaction between light-activated rhodopsin and the retinal G-protein transducin (G_t) as a model system. The interaction of activated rhodopsin with transducin has been well studied at a biochemical level by numerous methods and can be viewed as taking place in at least five discrete steps (Scheme 1). These include binding of R* to $G_{t\alpha\beta\gamma}$·GDP to form the R*·$G_{t\alpha\beta\gamma}$·GDP complex (steps 1 and 2), dissociation of GDP from the R*·$G_{t\alpha\beta\gamma}$·GDP complex to form an R*·$G_{t\alpha\beta\gamma}$[empty] complex (step 3), uptake of GTP by the R*·$G_{t\alpha\beta\gamma}$[empty] complex to form the R*·$G_{t\alpha\beta\gamma}$·GTP complex (step 4), and dissociation of $G_{t\alpha\beta\gamma}$·GTP from R* followed by $G_{t\alpha}$·GTP from $G_{t\beta\gamma}$ (step 5), with R* now available for interaction with another $G_{t\alpha\beta\gamma}$·GDP (*21*). Our previous studies have shown that an isotope-labeled G_α chimera (^{15}N-ChiT) can be isolated in a soluble, functional form that is amenable to structural analysis by solution NMR methods (*24*). ^{15}N-ChiT could also be reconstituted with $G_{t\beta\gamma}$ subunits to form a functional heterotrimer, with initial NMR measurements obtained for this reconstituted heterotrimer indicating that it may be "preactivated" or primed for R* interaction and guanine nucleotide exchange (ref *25* and Figure 1). Most recently (*26*), we have further demonstrated that high-resolution NMR methods can track guanine nucleotide exchange upon interaction of the ^{15}N-ChiT-reconstituted heterotrimer with light-activated rhodopsin (R*) and a soluble mimic of R* comprised of the second (CD) and third (EF) cytoplasmic loops of bovine opsin grafted onto a thioredoxin scaffold (HPTRX−CDEF). These latter studies highlighted our ability to interrogate GTPγS-bound forms of G_α that correspond to steps 4 and 5 in the reaction pathway (Scheme 1) and revealed that the process of guanine nucleotide exchange can be uncoupled from heterotrimer release and subunit dissociation.

Here, we have examined the conformation of G_α in the R*·$G_{\alpha\beta\gamma}$[empty] complex (Scheme 1, step 3, and Figure 1)

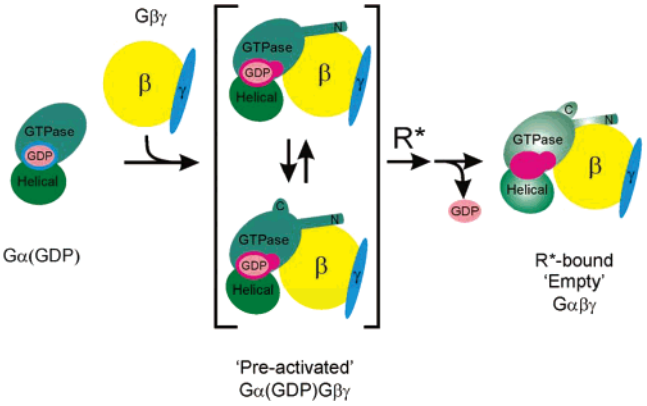

FIGURE 1: Model for heterotrimer-associated and R*-stimulated conformational changes in G_α. The GTPase and helical domains of G_α are colored different shades of green; G_β is colored yellow, and G_γ is colored blue. The region representing the guanine nucleotide-binding pocket in G_α is colored blue in the "ground" state and red in the preactivated state. GDP is colored salmon. Our previous NMR results (*25*) suggest that upon association of G_α(GDP) with $G_\beta\gamma$, G_α undergoes structural changes in the R*-interacting carboxyl-terminal region, as well as the switch regions surrounding the guanine nucleotide-binding pocket, and indicate that while $G_\beta\gamma$ binding changes the G_α structure to the preactivated form, it displays at least two conformational states for the carboxyl terminus. These changes in G_α structure may both potentiate R* interactions and preorganize the guanine nucleotide-binding pocket for subsequent binding of GTP. R* binds to the GDP-bound form of the G-protein ($G_{\alpha\beta\gamma}$[GDP]) and induces GDP release to form the nucleotide-free R*·$G_{\alpha\beta\gamma}$[empty] complex. In the empty pocket state following R*-catalyzed release of GDP, preorganization of the guanine nucleotide-binding pocket would facilitate GTP binding. Changes in the structure of the amino-terminal region of G_α are apparent from the crystal structures of the heterotrimer (*8*, *9*) and fluorescence and site-directed spin-labeling experiments (*55*), while changes in the carboxyl terminus are suggested from our NMR studies (*25*, *26*) and kinetic light scattering results (*21*).

using high-resolution NMR methods. This intermediate, "high-affinity" complex between R* and the nucleotide-free G-protein has been previously studied using the rhodopsin−G_t system in rod outer segment (ROS) membranes and has highlighted the reciprocal stabilizing interaction between R* and the G-protein (*27*). In fact, the stability of this intermediate complex has recently been quantified using plasmon-waveguide resonance measurements where a K_D for the R*−G_t interaction of ~1 nM has been reported (*28*). In this respect, it should be noted that this stable interaction forms the basis for a widely used G_t isolation procedure where the nucleotide-free heterotrimer is released from ROS membranes in the presence of GTP following extensive washing to remove contaminating proteins (*29*). Quite surprisingly, our NMR results suggest a dynamic, conformationally exchanged state of G_α in the R*·$G_{\alpha\beta\gamma}$[empty] complex that is formed through interactions with both light-activated rhodopsin and a soluble mimic of R*. In contrast to the conformational dynamics observed for G_α in the GDP-released R*-bound "empty pocket" state, GDP-depleted, Mg^{2+}-bound forms of G_α generated in isolation exhibit spectroscopic properties that are more closely aligned with those observed for the GDP/Mg^{2+}-bound form of G_α. These data imply that R*-induced changes in the receptor-interacting regions of G_α may be primarily responsible for the observed differences in G_α[empty] conformation and dynamics.

EXPERIMENTAL PROCEDURES[2]

Materials. The pG58 expression vector, a fusion vector encoding a modified 77-amino acid prodomain region of subtilisin BPN′ (proR8FKAM), and the pG58-derived expression vector encoding a G_α chimera [Chi6 (*30*)] as a proR8FKAM fusion have been described previously (*24*, *31*). The sources of other materials used in this investigation have been reported previously (*24*−*26*, *32*).

Expression and Purification of Subtilisin Prodomain−*Chi6 Fusions*. Methods for the inducible bacterial expression and purification of isotope-labeled wild-type and mutant G_α using the proR8FKAM−Chi6 fusion and immobilized S189 subtilisin BPN′ have been described previously (*24*). Prior to NMR analysis, the purified and isotope-labeled proteins were concentrated and dialyzed against 25 mM d_{11}-Tris-HCl (pH 7.5) containing 100 mM NaCl, 5 mM magnesium acetate, 2.5 mM DTT, and 5% glycerol (buffer A).

Preparation of GDP-Depleted ChiT. For generation of GDP-depleted ChiT, the proR8FKAM−Chi6 fusion was expressed and immobilized on S189 subtilisin BPN′ as described previously (*24*) except that GDP was omitted from the cell lysis and column purification buffers. The prodomain-released ChiT was then incubated in 25 mM Tris-HCl (pH 7.5) containing 100 mM NaCl, 10 mM EDTA, 5 mM β-mercaptoethanol, 5% glycerol, and 2.5 M urea for 30 min at 20 °C, followed by dialysis against 20 mM Tris-HCl (pH 7.5) containing 100 mM NaCl, 5 mM β-mercaptoethanol, and 5% glycerol to remove urea. Prior to fluorescence and NMR experiments, GDP-depleted ChiT was concentrated and dialyzed against buffer A. For reconstitution of GDP-depleted, Mg^{2+}-bound ChiT, the protein was incubated in the presence of GDP (100 μM) for 12−16 h at 4 °C prior to the acquisition of fluorescence and NMR data.

Reconstitution of ChiT with $G_{t\beta\gamma}$ To Form the $G_{\alpha\beta}$ Heterotrimer. G_t was isolated from frozen bovine retina and purified by GTP elution from washed ROS membranes as described previously (*29*, *33*). The G-protein heterotrimer was reconstituted from isotope-labeled ChiT and $G_{t\beta\gamma}$ essentially as described previously (*25*). Prior to NMR experiments, reconstituted heterotrimer preparations were concentrated and dialyzed against buffer A.

Detergent Solubilization and Purification of Rhodopsin. Rod outer segment (ROS) rhodopsin from bovine retina was solubilized and purified in Cymal-5 detergent on rho 1D4-Sepharose essentially as described previously (*26*). Rhodopsin concentrations were determined by UV−visible spectroscopy at 20 °C using a λ25 spectrophotometer (Perkin-Elmer Life and Analytical Sciences, Norwalk, CT). Prior to NMR experiments, rhodopsin preparations were concentrated and dialyzed against buffer A containing 0.08% Cymal-5.

Expression and Purification of HPTRX−*CDEF*. Detailed protocols for the inducible expression and purification of HPTRX−CDEF, a chimera containing segments from the CD and EF loops of bovine opsin grafted into a surface loop in thioredoxin, have been described previously (*32*). Prior to NMR experiments, purified HPTRX−CDEF was concentrated and dialyzed against buffer A.

Fluorescence Assay for Measuring R Decay in the Absence and Presence of G_t*. The rate of R* decay for Cymal-5 solubilized and purified rhodopsin in the absence and presence of G_t was measured essentially as described by Farrens and Khorana (*34*) for DM solubilized and purified rhodopsin. Briefly, purified rhodopsin (250 nM) in 25 mM Tris-HCl (pH 7.5) containing 100 mM NaCl, 5 mM magnesium acetate, 2.5 mM DTT, 5% glycerol, and 0.08% Cymal-5 was incubated in the absence or presence of G_t (300 nM) in a 1 cm square quartz cuvette for 40 min at 25 °C and illuminated (>495 nm) for 30 s, and the intrinsic fluorescence accompanying R* decay was monitored in signal/reference mode using a TimeMaster spectrofluorometer (Photon Technology International, Birmingham, NJ) for up to 500 min. Excitation was at 295 nm, and emission was recorded at 330 nm. The spectral excitation band-pass was 2 nm and the emission 10 nm. The signal integration time was set at 1 s. In the assay mixture with rhodopsin and G_t, GTPγS (2.5 μM) was added ~800 min following illumination of the sample. Data analysis was performed using SigmaPlot version 9.0.

Fluorescence Assay for Measuring AlF_4^--Dependent Changes in ChiT. The tryptophan fluorescence of the GDP/Mg^{2+}-bound and empty pocket forms of ChiT in the absence and presence of AlF_4^- was determined in signal/reference mode essentially as described previously (*25*) using a FluoroMax-3 spectrofluorometer (Instruments SA, Edison, NJ) with a 0.3 cm square cuvette at 20 °C. In all cases, AlF_4^- was added as a premixed solution (final concentrations of 3 μM $AlCl_3$ and 0.3 mM NaF). Emission spectra were recorded over the wavelength range of 310−450 nm with an excitation wavelength of 290 nm. The spectral excitation and emission band-pass was 5 nm for all spectra, with a signal integration time of 1 s. Data analysis was performed using SigmaPlot version 9.0.

Fluorescence and Filter Binding G_t Activity Assays. The functionality of the R*-bound nucleotide-free G-protein heterotrimer was examined using a fluorescence assay for R*-catalyzed G-protein activation as described previously (*32*), which has been modified from previously reported methods (*35*, *36*). This assay allows measurement of the rate and extent of uptake of GTPγS by G_α by monitoring the increase in intrinsic fluorescence of Trp-207 (*37*). Briefly, purified rhodopsin (250 nM) in 25 mM Tris-HCl (pH 7.5) containing 100 mM NaCl, 5 mM magnesium acetate, 2.5 mM DTT, 5% glycerol, and 0.08% Cymal-5 was incubated with G_t (300 nM) for 40 min at 25 °C in the dark. The sample was then illuminated (>495 nm) for 1 min at 25 °C to form the R*·$G_{\alpha\beta\gamma}$[empty] complex. At defined time periods, aliquots were removed and transferred to a 1 cm square quartz cuvette, and the change in the intrinsic G_α fluorescence following addition of GTPγS (2.5 μM) was monitored in signal/reference mode using a Cary Eclipse spectrofluorometer (Varian Inc., Palo Alto, CA) for up to 32 h. Excitation was at 310 nm, and emission was recorded at 345 nm. The spectral excitation and emission band-pass was set at 10 nm with a signal integration time of 1 s. Both the initial rate and peak signal amplitude data were analyzed and compared at the various time points. In addition, the functionality of the R*-bound nucleotide-free G-protein heterotrimer was

[2] Certain commercial equipment, instruments, and materials are identified in this paper to specify the experimental procedure. Such identification does not imply recommendation or endorsement by the National Institute of Standards and Technology, nor does it imply that the material or equipment identified is necessarily the best available for the purpose.

examined by following the R*-catalyzed uptake of [^{35}S]-GTPγS using a nitrocellulose filter binding assay (*38*) essentially as described previously (*39*). The filter binding assay is based on the property that G_α and its bound [^{35}S]-GTPγS are retained on nitrocellulose filters, whereas free [^{35}S]GTPγS passes through the filters. Briefly, a sample mixture identical to that to that prepared above for the fluorescence assay was illuminated (>495 nm) for 1 min at 25 °C to form the R*·$G_{\alpha\beta\gamma}$[empty] complex. At defined time periods (2−32 h), an aliquot was removed and added to a solution of [^{35}S]GTPγS (2.5 μM). After 20 min at 25 °C, duplicate samples were filtered through nitrocellulose, the filters were washed at least five times with 10 mL of 25 mM Tris-HCl (pH 7.5) containing 100 mM NaCl, 5 mM magnesium acetate, 2.5 mM DTT, and 5% glycerol, and dried, and bound radioactivity was quantified by scintillation counting. The level of light-dependent [^{35}S]GTPγS binding was analyzed and compared at the various time points. Data analysis was performed using SigmaPlot version 9.0.

HPLC Analysis of Guanine Nucleotides. Chromatographic analysis of bound guanine nucleotides in the different ChiT preparations was performed essentially as described previously (*40*). Briefly, ChiT (400 μg) prepared in the absence or presence of GDP was denatured in 100 mM phosphate buffer (pH 6.5) containing 10 mM tetrabutylammonium bromide, 7.5% acetonitrile, and 0.2 mM NaN_3 (buffer B). The samples were centrifuged at 12000*g* for 10 min to remove denatured protein, and the supernatant was applied to an Xterra MS C-18 reverse phase column (Waters Corp., 2.5 μm pore size, 10 mm × 50 mm). Prior to sample loading, the column was equilibrated with buffer B and calibrated with a 200 μM solution of GDP in buffer B.

NMR Spectroscopy. One-dimensional (1D) ^{15}N-filtered and two-dimensional (2D) ^{15}N heteronuclear single-quantum correlation (HSQC) water flip-back, water gate experiments (*41*) were conducted at 30 °C on a Bruker AVANCE 600 MHz spectrometer (Bruker Instruments, Billerica, MA) equipped with either a triple-resonance ^{1}H, ^{13}C, ^{15}N *Z*-axis gradient cryoprobe or a conventional, triple-resonance ^{1}H, ^{13}C, ^{15}N triple-axis gradient probe and linear amplifiers on all three channels. For all spectra, the nitrogen frequency was centered at 118 ppm and the proton frequency on H_2O (~7.5 ppm). NMR samples containing rhodopsin and ^{15}N-ChiT reconstituted heterotrimer in equimolar amounts (150 μM) were dialyzed against buffer A containing 0.08% Cymal-5 and initially placed in the spectrometer under dim-red light conditions for acquisition of reference "dark" spectra. To trigger formation of the R*−G-protein complex and GDP release, the sample was illuminated with >495 nm light for 1 min prior to spectral acquisition. 1D spectra were collected using a sweep width of 7200 Hz and 2K complex points, while 2D data were collected using sweep widths of 7200 Hz in ω_2 and 2000 Hz in ω_1, 2K and 24 complex data points in t_2 and t_1, respectively (t_{1max} = 293 ms and t_{2max} = 12 ms), and 400 scans per increment. The total measurement time was ~8.5 h. For NMR samples containing HPTRX−CDEF, the protein was titrated directly with the ^{15}N-ChiT reconstituted heterotrimer to form the 1:1 complex (~150 μM) and stimulate GDP release. For this complex, 1D spectra were again collected using a sweep width of 7200 Hz and 2K complex points, while 2D data were collected using sweep widths of 7200 Hz in ω_2 and 2000 Hz in ω_1, 2K and 32 complex data points in t_2 and t_1, respectively (t_{1max} = 293 ms and t_{2max} = 12 ms), and 320 scans per increment. The total measurement time was ~9.5 h. Spectra were acquired for the GDP-depleted, Mg^{2+}-bound ^{15}N-ChiT sample (250 μM) in buffer A. 1D spectra were collected using a sweep width of 7200 Hz and 2K complex points, while 2D data were collected using sweep widths of 7200 Hz in ω_2 and 2000 Hz in ω_1, 2K and 64 complex data points in t_2 and t_1, respectively (t_{1max} = 293 ms and t_{2max} = 32 ms), and 128 scans per increment. The total measurement time was ~4 h. All spectra were processed using the same processing functions and analyzed on a PC/LINUX workstation using NMRPipe (*42*). The ^{15}N HSQC spectra of ^{15}N-ChiT in its GDP/Mg^{2+}-bound, heterotrimer-reconstituted, and HPTRX−CDEF-exchanged forms, which are used as references for comparisons, were acquired as previously described (*24*−*26*). Trp indole and Phe-350 amide ^{1}NH and ^{15}N resonances were assigned using ChiT mutants also as previously described (*24*−*26*).

Other Methods. Analysis of protein samples by SDS−PAGE and protein determinations were carried out as previously described (*26*).

RESULTS

Trapping an R·$G_{\alpha\beta\gamma}$[empty] Complex*. We have previously shown that solution NMR can be used to track the cycle of guanine nucleotide exchange in an isotope-labeled G_α reconstituted heterotrimer that is triggered by detergent-solubilized, light-activated rhodopsin (R*), and that NMR measurements can provide new insights into G_α conformational changes associated with signal propagation from an activated GPCR (*26*). Solution NMR methods have similarly been used to track guanine nucleotide exchange stimulated by a soluble mimic of R*, HPTRX−CDEF, that remains bound to the exchanged heterotrimer forming a trapped, stable complex. The observations from these studies have provided evidence to suggest that guanine nucleotide exchange can be uncoupled from the process of heterotrimer release and subunit dissociation (*26*). In both of these NMR studies, to simulate the reaction scheme of the R*−G-protein interaction which leads to the formation and dissociation of the R*·$G_{\alpha\beta\gamma}$·GTP complex (Scheme 1, steps 4 and 5), the nonhydrolyzable GTP analogue GTPγS was included in the experimental protocol. Here, GTPγS has been omitted to "trap" the R*−G-protein interaction at the empty pocket state (Scheme 1, step 3).

Stability of the R·$G_{\alpha\beta\gamma}$[empty] Complex in Cymal-5 Detergent.* Rhodopsin in 0.08% Cymal-5 detergent interacts with G_t to form a complex that triggers guanine nucleotide exchange (*25*, *26*). To examine the stability of R* in the R*·$G_{\alpha\beta\gamma}$[empty] complex at this detergent concentration, the rate of R* decay in the absence and presence of G_t was monitored using a well-established intrinsic tryptophan fluorescence assay for retinal release (*34*). As shown in Figure 2A, illumination of rhodopsin results in a time-dependent increase in the intrinsic tryptophan fluorescence as a consequence of R* decay, which reflects the release of all-*trans* retinal from the opsin apoprotein. In the presence of G_t, this increase in fluorescence was greatly diminished because of the formation of the GDP-released R*·$G_{\alpha\beta\gamma}$-[empty] complex, which traps or maintains R* in the retinal-

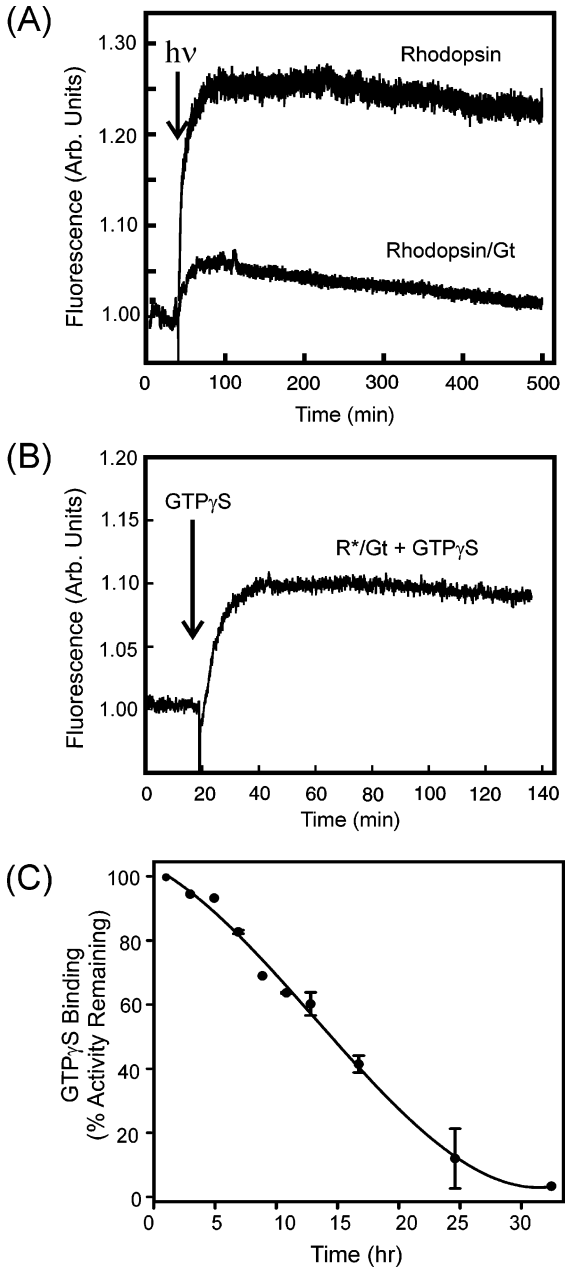

FIGURE 2: Stability of the R*·$G_{\alpha\beta\gamma}$[empty] complex in Cymal-5. (A) R* decay in the absence and presence of G_t. The time-dependent increase in fluorescence at 330 nm as a consequence of release of retinal from the opsin apoprotein is diminished in the presence of G_t due to the formation of the GDP-released R*·$G_{\alpha\beta\gamma}$[empty] complex which traps R* in the retinal-bound conformation. (B) Binding of GTPγS to the R*·$G_{\alpha\beta\gamma}$ complex. GTPγS was added ~800 min after complex formation, and the time-dependent increase in fluorescence at 330 nm was monitored for an additional ~100 min. Under the conditions of this assay, the observed fluorescence changes report on both guanine nucleotide uptake by G_α and retinal release from R* accompanying dissolution of the complex. In panels A and B, fluorescence spectra were acquired as described in ref *33* as described in Experimental Procedures. Representative traces from two or three independent determinations are shown. (C) G_t activity in the R*·$G_{\alpha\beta\gamma}$[empty] complex. G-Protein activity was followed by monitoring the change in fluorescence at 345 nm following addition of GTPγS to the R*·$G_{\alpha\beta\gamma}$[empty] complex. Data points reflect the peak signal amplitude achieved at the time GTPγS was added following formation of the complex. Fluorescence spectra were acquired according to ref *32*, as described in Experimental Procedures. Results from two independent determinations are shown as averages ± the standard error.

bound conformation (*27*). The observed initial increase in fluorescence following illumination in the presence of G_t, which decreases to near baseline over the course of the experiment, may reflect the decay of R* that did not effectively form a complex with G_t, a change in the conformation of $G_{t\alpha}$ as a consequence of GDP release, which could alter the environment of Trp-207 (*37*), or a combination of both. Since similar initial rates can be fit for the two curves, it appears that the observed increase in intrinsic fluorescence following illumination in the presence of G_t is due to a minor population of R* that did not form a complex. These findings are qualitatively similar to what we observed previously using a UV−visible spectroscopic assay for R* decay that showed conversion to opsin and free all-*trans* retinal was significantly reduced in the presence of G_t with greater than ~80% of the R* remaining after 8 h (*26*).

To examine the functionality of the G-protein in the R*·$G_{\alpha\beta\gamma}$[empty] complex, we initially added GTPγS ~800 min after illumination. As shown in Figure 2B, this resulted in a significant enhancement of the intrinsic fluorescence when monitored under conditions of the retinal release assay. However, as this increase may reflect changes in the intrinsic fluorescence of both rhodopsin (R* decay) and $G_{t\alpha}$ (uptake of GTPγS) accompanying guanine nucleotide uptake and dissolution of the complex, a more thorough and comparative analysis of G-protein functionality in the complex was conducted using a fluorescence assay that more closely reports on intrinsic fluorescence changes at Trp-207 in G_α accompanying GTPγS uptake (*32*, *35*−*37*). The results of this assay showed that ~70−75% of the nucleotide-free G-protein remains competent for GTPγS binding in the R*·$G_{\alpha\beta\gamma}$[empty] complex for a period of up to 8−8.5 h, slightly shorter than what has been previously determined for R* in the presence of G_t (*26*). Under these assay conditions, the half-life of G_t in the R*·$G_{\alpha\beta\gamma}$[empty] complex corresponds to ~13 h. Comparable results were obtained using a radioactive filter binding assay (data not shown). Collectively, these results indicate that both R* and the G-protein in the R*·$G_{\alpha\beta\gamma}$[empty] complex largely remain in a functional form on a time scale that is compatible with the acquisition of NMR data.

Light-Activated Rhodopsin (R)-Catalyzed Formation of Empty Pocket ^{15}N-Labeled ChiT Reconstituted Heterotrimer*. To characterize the structure of G_α in the R*·$G_{\alpha\beta\gamma}$[empty] complex, an experimental protocol similar to that outlined for light-activated rhodopsin-catalyzed generation of the GTPγS/Mg^{2+}-bound form of ^{15}N-ChiT (*26*) was utilized. In this case, however, stoichiometric amounts (~150 μM) of rhodopsin (~40 kDa) and ^{15}N-ChiT reconstituted heterotrimer (~85 kDa) were incubated in the absence of GTPγS and then illuminated for 1 min at >495 nm. 1D ^{15}N-filtered ^{1}H and 2D HSQC spectra were then immediately acquired after the sample had been placed into the NMR spectrometer to assay the conformation of ^{15}N-ChiT in the R*·$G_{\alpha\beta\gamma}$[empty] complex. 1D spectra acquired within the first few minutes of the illuminated sample being placed into the spectrometer exhibited a decrease in signal intensity and changes in chemical shifts for the ^{15}N-filtered ChiT resonances that would be expected upon formation of the R*·$G_{\alpha\beta\gamma}$[empty] complex (data not shown). A HSQC spectrum of the R*-bound empty pocket ^{15}N-ChiT reconstituted heterotrimer was then acquired after the initial 1D data and is shown in Figure

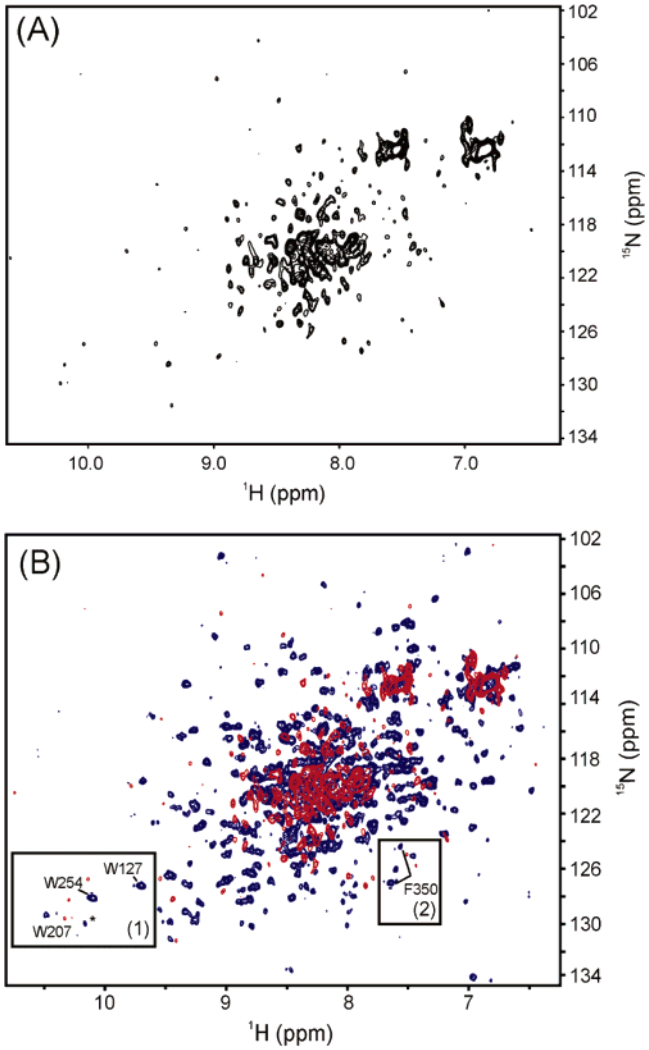

FIGURE 3: HSQC spectra acquired for the ^{15}N-ChiT reconstituted heterotrimer in the light-activated rhodopsin-bound empty pocket and GDP/Mg^{2+}-bound states. (A) Amide region of the 2D HSQC spectrum of ChiT in the R*·$G_{\alpha\beta\gamma}$[empty] complex. (B) Overlay of the amide region of the 2D HSQC spectrum of ChiT in the R*·$G_{\alpha\beta\gamma}$[empty] complex (red) and in the GDP/Mg^{2+}-bound form of the heterotrimer (blue). In panel B, the assigned ^{1}HN−^{15}N cross-peaks for the Trp indoles (Trp-127, Trp-207, and Trp-254) are shown in box 1 and those for the carboxyl-terminal Phe-350 residue in box 2. The difference in the conformation of ChiT in these two heterotrimer states is primarily manifested by the severe exchange broadening of ^{1}HN−^{15}N cross-peaks of ChiT in the R*·$G_{\alpha\beta\gamma}$[empty] complex when compared to the GDP/Mg^{2+}-bound form of the heterotrimer. Spectra were acquired as described in Experimental Procedures. Note that the extended line shapes observed for ^{15}N cross-peaks of ChiT in the R*·$G_{\alpha\beta\gamma}$[empty] complex in the inverse dimension are due in part to the fact that this data set was acquired with fewer ω_1 points relative to the spectra of ChiT in the GDP/Mg^{2+}-bound form of the heterotrimer.

3A. It should be noted that in this spectrum, only the subset of backbone amide and side chain indole/amino resonances from ^{15}N-ChiT is selectively observed. Unlike previous ^{15}N HSQC spectra acquired for the various guanine nucleotide-bound states of ChiT (*24*−*26*), including the GDP/Mg^{2+}-bound form of the heterotrimer (see overlay in Figure 3B), the R*-bound empty pocket state shows severe broadening of amide resonances that suggest the formation of a metastable dynamic structure. It should be emphasized that the spectrum of this R*-bound state of G_α does not represent an unfolded or aggregated, nonfunctional state of G_α, as subsequent addition of GTPγS leads to the generation of a stabilized guanine nucleotide-exchanged state of ChiT that is indistinguishable from the GTPγS/Mg^{2+}-bound form of ChiT generated by inclusion of GTPγS during the course of the guanine nucleotide exchange reaction (*26*).

HPTRX−*CDEF Stimulated Formation of Empty Pocket ^{15}N-Labeled ChiT Reconstituted Heterotrimer.* We have previously shown that the HPTRX−CDEF fusion protein (~15 kDa), which contains tandemly linked segments from the CD (amino acids 132−154) and EF (amino acids 231−252) loops of rhodopsin grafted onto a thioredoxin scaffold (*32*), forms a stoichiometric complex with the G-protein to stimulate guanine nucleotide exchange but does not appear to release the GTPγS/Mg^{2+}-exchanged heterotrimer (*26*). These results provide an explanation for the observation that while HPTRX−CDEF stimulates guanine nucleotide exchange with kinetic rates that are almost indistinguishable from that of R*, it does not catalytically interact with G_t. Since the GTPγS/Mg^{2+}-bound state of G_α in the ^{15}N-ChiT reconstituted heterotrimer bound to HPTRX−CDEF shares many similarities with the GTPγS/Mg^{2+}-bound state of G_α in isolation, including an "activated" guanine nucleotide-binding pocket and carboxyl terminus (*26*), this raised the prospect that HPTRX−CDEF may also stimulate guanine nucleotide exchange through a mechanism similar to that of R* by proceeding through an empty pocket intermediate. As might be anticipated on the basis of its ability to stimulate guanine nucleotide exchange (*26*, *32*), HPTRX−CDEF also appears to proceed through an empty pocket state that could be transiently generated through the addition of HPTRX−CDEF (~150 μM) to ^{15}N-ChiT reconstituted heterotrimer (~150 μM) in the absence of GTPγS. Figure 4A shows the 1D ^{15}N-filtered spectra acquired as ^{15}N-ChiT reconstituted heterotrimer was titrated with HPTRX−CDEF. These spectra exhibit proportional decreases in signal intensity and changes in chemical shifts for the ^{15}N-filtered ChiT resonances as might be expected upon formation of a 1:1 stoichiometric complex between HPTRX−CDEF and $G_{\alpha\beta\gamma}$[empty]. A HSQC spectrum of the HPTRX−CDEF-bound empty pocket ^{15}N-ChiT reconstituted heterotrimer acquired after addition of an equimolar amount of HPTRX−CDEF to ^{15}N-ChiT reconstituted heterotrimer is shown in Figure 4B. Like the light-activated rhodopsin-generated empty pocket state of the heterotrimer (Figure 3A), the HPTRX−CDEF-generated empty pocket state of ChiT also shows severe broadening of resonances that again suggests a significant degree of conformational exchange likely due to the formation of a dynamic intermediate structure and/or interaction. Interestingly, the degree of line broadening resulting from formation of the HPTRX−CDEF-bound empty pocket ^{15}N-ChiT reconstituted heterotrimer appears to be even more severe than for detergent-solubilized R*. This observation may result from the absence of additional "stabilizing" contacts in the HPTRX−CDEF-bound complex that are likely present in the R*−G-protein interaction.

Taken together, the observations of line broadening for the majority of ^{15}N-ChiT resonances under two significantly different experimental protocols (i.e., in the presence of a detergent-solubilized receptor or a soluble fusion protein) suggest that this results from a change in the intrinsic dynamic nature of this intermediate R*-bound state of G_α

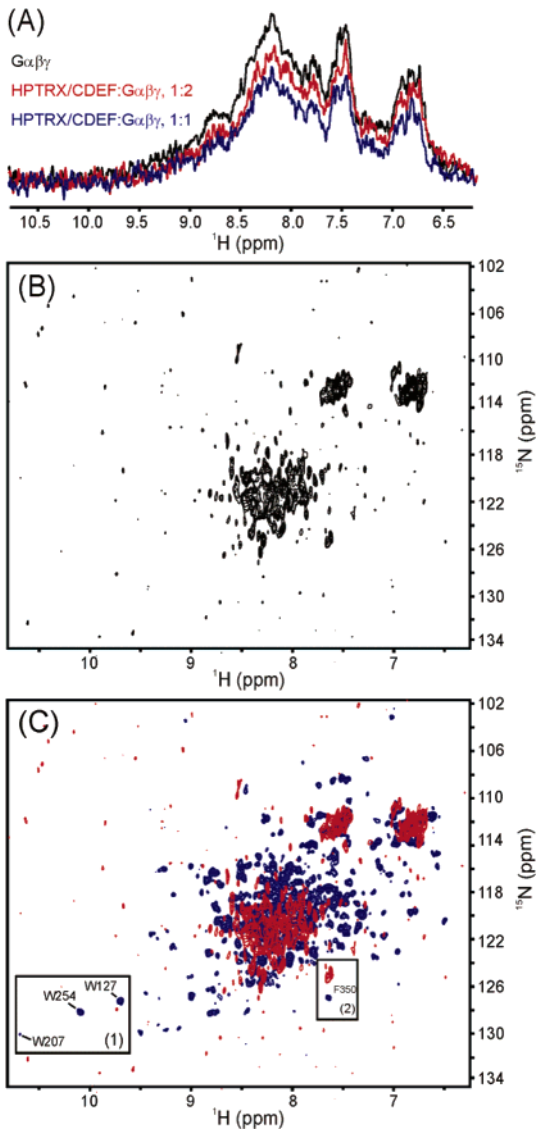

FIGURE 4: HPTRX−CDEF-stimulated formation of empty pocket ^{15}N-ChiT reconstituted heterotrimer. (A) Titration of the ^{15}N-ChiT reconstituted heterotrimer with HPTRX−CDEF. Expansions of the amide region (from 10.8 to 6.0 ppm) of 1D ^{15}N-filtered proton spectra are shown for ^{15}N-ChiT reconstituted heterotrimer (150 μM) and ^{15}N-ChiT reconstituted heterotrimer in the presence of 0.5 and 1.0 molar equiv of unlabeled HPTRX−CDEF. (B) Amide region of the HSQC spectra acquired for the ^{15}NChiT reconstituted heterotrimer in the HPTRX−CDEF·$G_{\alpha\beta\gamma}$[empty] complex. (C) Overlay of the amide region of the 2D HSQC spectrum of ChiT in the HPTRX−CDEF·$G_{\alpha\beta\gamma}$[empty] complex (red) and in the HPTRX−CDEF·$G_{\alpha\beta\gamma}$·GTPγS/Mg^{2+}-exchanged complex (blue). In panels B and C, the assigned ^{1}HN−^{15}N cross-peaks for the Trp indoles (Trp-127, Trp-207, and Trp-254) are shown in box 1 and those for the carboxyl-terminal Phe-350 residue in box 2. The difference in the conformation of ChiT in these two heterotrimer states is manifested primarily by a severe broadening of resonances in the HPTRX−CDEF-bound empty pocket state of ChiT in the reconstituted heterotrimer relative to the HPTRX−CDEF·$G_{\alpha\beta\gamma}$·GTPγS/Mg^{2+}-exchanged complex. As in the R*·$G_{\beta\gamma}$[empty] complex (Figure 3), the observation of exchange broadening of ChiT resonances in the HPTRX−CDEF·$G_{\alpha\beta\gamma}$[empty] complex suggests that ChiT adopts a conformationally dynamic structure here as well. Spectra were acquired as described in Experimental Procedures. Note that the extended line shapes generally observed for ^{15}N cross-peaks of ChiT in the HPTRX−CDEF-bound empty pocket state of ChiT in the inverse dimension are due in part to the fact that this data set was acquired with fewer ω_1 points relative to the spectra of ChiT in the HPTRX−CDEF·$G_{\alpha\beta\gamma}$·GTPγS/Mg^{2+}-exchanged complex.

and not from a more trivial effect such as protein aggregation or unfolding. In addition, as shown by the overlay of the amide region of ^{15}N-ChiT in the HPTRX−CDEF·$G_{\alpha\beta\gamma}$-[empty] complex and in the HPTRX−CDEF·$G_{\alpha\beta\gamma}$·GTPγS/Mg^{2+}-exchanged complex (Figure 4C), addition of GTPγS restores ChiT to a less dynamic state. Since the resulting trapped HPTRX−CDEF·$G_{t\alpha\beta\gamma}$·GTPγS-exchanged complex displays a reasonably disperse and sharper HSQC spectrum, this again suggests that the broadening of resonances in the R*-bound empty pocket heterotrimer states is not simply due to the increase in size of the complexes (at least ~100 kDa in the case of HPTRX−CDEF and ~125 kDa for rhodopsin), but again to be predominately the result of a change in the dynamic nature of this transiently formed state of G_α.

*AlF_4^--Dependent Tryptophan Fluorescence Changes in GDP-Depleted ChiT Generated in a Manner Independent of R**. To analyze the conformation of the G_α subunit in the absence of bound guanine nucleotide, a GDP-depleted form of ChiT was prepared by disrupting the cells in buffer devoid of GDP followed by a brief treatment with urea to remove any residual bound endogenous GDP from the prodomain-released G_α. After dialysis, HPLC analysis of ChiT generated using this approach showed that >95% of the G_α could be routinely isolated in a guanine nucleotide-free state (Figure 5A). As would be expected if G_α contained little or no bound GDP, addition of AlF_4^- resulted in no significant change in Trp-207 fluorescence (Figure 5B). However, reconstitution of this form of G_α with GDP, followed by addition of AlF_4^-, resulted in a considerable increase in Trp-207 fluorescence (Figure 5C), similar to the level of enhancement (~30−35%) observed for the GDP/Mg^{+2}-bound form of ChiT (Figure 5C, inset). These results suggest that ChiT can be isolated in an essentially nucleotide-free state and that this form of G_α retains the capacity to bind GDP in a functional manner.

NMR Analysis of GDP-Depleted, Mg^{2+}-Bound ^{15}N-ChiT. To characterize the conformation of G_α in the absence of bound guanine nucleotide, a ^{15}N HSQC spectrum of GDP-depleted, Mg^{2+}-bound ^{15}N-ChiT was acquired (Figure 6A). Interestingly, a comparison of the amide region of the HSQC spectrum of the GDP-depleted form of ChiT generated in a manner independent of R* and ChiT in the R*·$G_{\alpha\beta\gamma}$[empty] complex (Figures 3A and 6A) shows that these two states exhibit very different amide resonance line widths, with the empty pocket form of ChiT generated in a manner independent of R* displaying a spectrum with only relatively modest line broadening. Furthermore, a comparison of the HSQC spectra for the GDP-depleted, Mg^{2+}-bound, and GDP/Mg^{2+}-bound forms of ^{15}N-ChiT (Figure 6B) shows that both of these states of ChiT have similar amide resonance chemical shifts, although line widths for some of the ^{1}HN−^{15}N correlations observed in the GDP-depleted, Mg^{2+}-bound state of the protein are broader than in the GDP/Mg^{2+}-bound state. The GDP-depleted, Mg^{2+}-bound form of ChiT also displays chemical shift positions for the Trp indole ^{1}HN−^{15}N resonances that are similar to those of the GDP/Mg^{2+}-bound state of ChiT, suggesting a similar conformation for the switch II and α_3/β_5 regions in the absence of bound GDP (Figure 6B). After reconstitution of the same ChiT sample with GDP and subsequent addition of AlF_4^- (Figure 6C, left panel), the ^{15}N−^{1}HN cross-peaks for the Trp-127 and Trp-254 indole resonances are observed to shift to the same positions as previously reported (*24*−*26*), while in

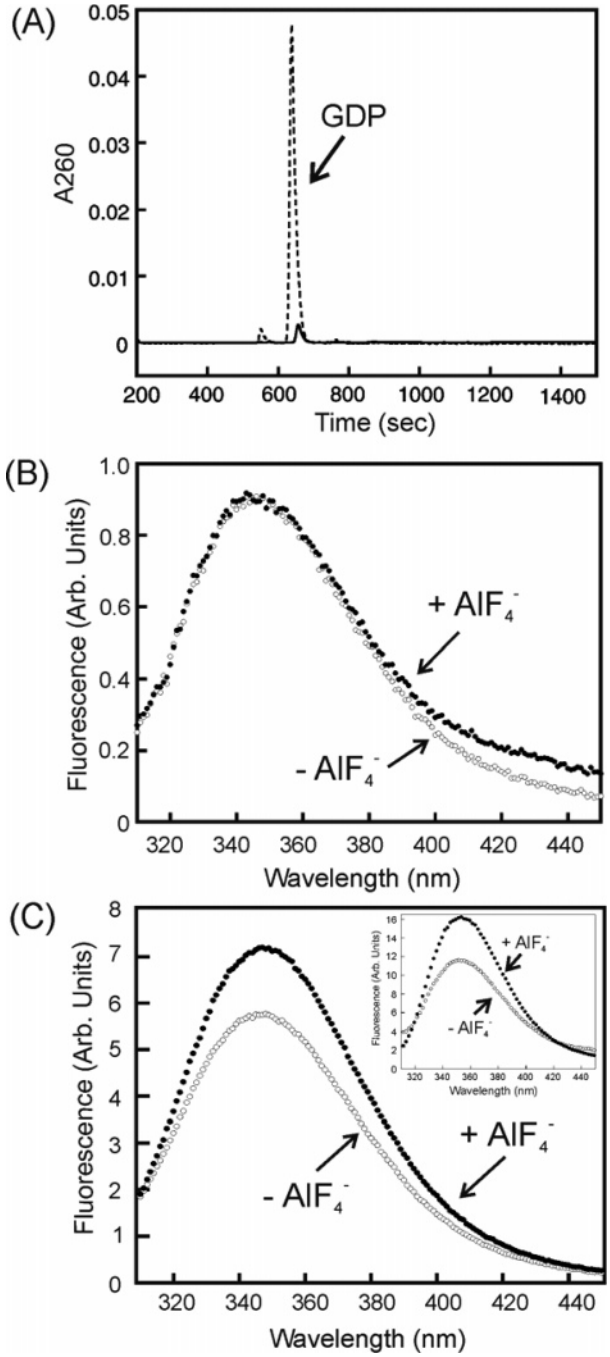

FIGURE 5: Properties of GDP-depleted, Mg^{2+}-bound ChiT. (A) HPLC analysis of the GDP-depleted, Mg^{2+}-bound, and GDP/Mg^{2+}-bound forms of ChiT. ChiT samples were denatured in phosphate buffer containing 7.5% acetonitrile in 10 mM tetrabutylammonium bromide to release any bound guanine nucleotide, and the supernatant obtained after centrifugation was chromatographed on a C-18 reverse phase column as described in Experimental Procedures. The results of this analysis for the GDP-depleted, Mg^{2+}-bound, and GDP/Mg^{2+}-bound forms of ChiT are shown in solid and dashed traces, respectively. A solution of 200 μM GDP was used as a standard. Fluorescence changes accompanying AlF_4^- treatment of the GDP-depleted, Mg^{2+}-bound form of ChiT before (B) and after (C) reconstitution with GDP. Emission spectra for GDP-depleted, Mg^{2+}-bound ChiT or GDP/Mg^{2+}-reconstituted ChiT in the absence (○) and presence (●) of AlF_4^- (final concentrations of 3 μM $AlCl_3$ and 0.3 mM NaF) were determined as described in Experimental Procedures. The inset of panel C shows emission spectra for the GDP/Mg^{2+}-bound form of ChiT before (○) and after (●) the addition of AlF_4^- using the same experimental parameters. Representative traces from two or three independent determinations are shown.

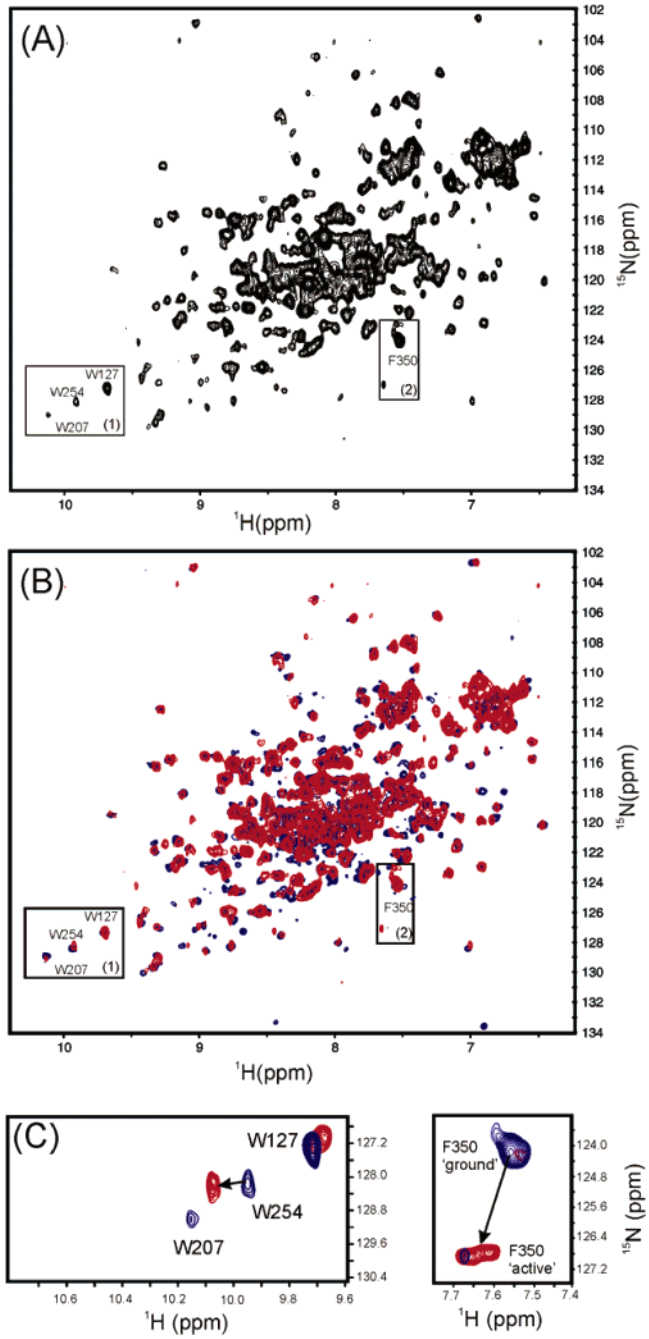

FIGURE 6: Comparison of HSQC spectra acquired for ^{15}N-ChiT in the GDP/Mg^{2+}-bound and GDP-depleted, Mg^{2+}-bound states. (A) Amide region of the 2D HSQC spectrum of the GDP-depleted, Mg^{2+}-bound form of ChiT. The assigned ^{1}HN−^{15}N cross-peaks for the three Trp indoles (Trp-127, Trp-207, and Trp-254) are shown in box 1, and that for the carboxyl-terminal Phe-350 residue is shown in box 2. (B) Overlay of the amide region of the 2D HSQC spectrum of the GDP-depleted, Mg^{2+}-bound form of ChiT generated in a manner independent of R* (red) and the GDP/Mg^{2+}-bound form of ChiT (blue). ChiT displays striking similarities in the chemical shifts of the ^{1}HN−^{15}N cross-peaks for these two different states. The assigned ^{1}HN−^{15}N cross-peaks for the three Trp indoles (Trp-127, Trp-207, and Trp-254) are shown in box 1, and that for the carboxyl-terminal Phe350 residue is shown in box 2. (C) Comparison of the ^{1}HN−^{15}N correlations of the Trp indoles (left panel) and Phe-350 (right panel) for the GDP-depleted, Mg^{2+}-bound form of ChiT (blue), and after reconstitution of the same ChiT sample with GDP and subsequent addition of AlF_4^- (red). Assignments for the ^{1}HN−^{15}N cross-peaks are indicated, and differences in chemical shifts between the various states of ChiT for the ^{1}HN−^{15}N correlations are highlighted. Spectra were acquired as described in Experimental Procedures.

contrast, the indole resonance for Trp-207 appears to be exchange broadened beyond detection. It is worth noting that exchange broadening of this resonance was previously observed in the GTPγS/Mg^{2+}-bound form of ChiT generated through interactions of the ^{15}N-ChiT reconstituted heterotrimer with R* in the presence of GTPγS. In addition, the chemical shift position of the amide $^{15}N-^{1}HN$ cross-peak of Phe-350 in this state of G_α is also the same as previously observed in the GDP/Mg^{2+}-bound state of ChiT (Figure 6C, right panel), while after reconstitution of the same ChiT sample with GDP and subsequent addition of AlF_4^-, the chemical shift position of Phe-350 is observed to similarly shift to the previously described activated position. However, in the case of GDP/Mg^{2+}-reconstituted ChiT, two cross-peaks are observed upon addition of AlF_4^-, indicating that at least two states exist for this activated conformation of the carboxyl terminus that are relatively equally populated and in slow exchange. Overall, these observations demonstrate that while the R*-bound empty pocket state of the heterotrimer-associated G_α is characterized by conformational exchange, the GDP-depleted, Mg^{2+}-bound state of G_α in isolation is largely characterized by a conformation that, while dynamic, shares many features with Gα(GDP). This suggests that the presence of guanine nucleotide in the binding pocket is not a primary factor contributing to G_α conformation and stability.

In summary, these results show that both light-activated rhodopsin and a soluble mimic of R* form trapped intermediate complexes with an empty pocket state of the heterotrimer in the absence of GTPγS. Comparisons of the R*-generated empty pocket state of G_α with various guanine nucleotide-bound forms of the protein indicate that this state is conformationally dynamic and likely represents a metastable intermediate. Interestingly, the conformation of a GDP-depleted, Mg^{2+}-bound state of G_α formed in a manner independent of R* does not exhibit a similar degree of conformational dynamics but rather appears structurally similar to the GDP/Mg^{2+}-bound form of the protein. Overall, our results suggest that changes in the R*-interacting regions of G_α, and not the absence of bound guanine nucleotide, are the predominant factors governing the G_α conformation and dynamics in the R*-bound empty pocket state.

DISCUSSION

A number of different proposals have been put forth to explain how structural changes in the R*-interacting regions of a heterotrimeric G-protein may lead to GDP release and GTP uptake (*18*−*23*). In all of these proposals, the R*-bound empty pocket form of the heterotrimer is a key intermediate in the reaction mechanism. Evidence in support of its existence as an intermediate high-affinity complex between R* and the G-protein was first discerned from the early work of Kühn and subsequently investigated in detail by Chabre and co-workers (*28*, *29*). In the latter work, it was shown that in the R*·$G_{\alpha\beta\gamma}$[empty] complex formed in ROS membranes, G_t retains the ability to bind both GDP and GTP while R* (metarhodopsin II) remains spectroscopically stable (i.e., does not decay to opsin and free all-*trans* retinal). These results suggested a reciprocal interaction between the chromophore binding site in R* and the guanine nucleotide-binding pocket in $G_{t\alpha}$. In our study, such findings have been extended to the R*·$G_{\alpha\beta\gamma}$[empty] complex in detergent solution as the binding of G_t to R* in 0.08% Cymal-5 diminishes the rate of retinyl-Schiff base hydrolysis by prolonging the lifetime of R*, with the R*-bound heterotrimer remaining competent for GTPγS uptake (Figure 2). The R*·$G_{\alpha\beta\gamma}$[empty] complex has also been characterized by limited proteolysis, primarily susceptibility to trypsin (*43*). Here, the formation of defined fragments of $G_{t\alpha}$ was retarded upon incubation of the R*·$G_{\alpha\beta\gamma}$[empty] complex with trypsin, when compared with fragments of $G_{t\alpha}$ in the heterotrimer in isolation or in the presence of ROS membranes not exposed to light. Bubis et al. (*44*) have also shown that carboxymethylation of Cys-347 in $G_{t\alpha}$ stabilizes the R*·$G_{\alpha\beta\gamma}$[empty] complex, suggesting that the extreme carboxyl terminus of G_α, a known R*-interacting region, may be involved in facilitating GTP uptake.

The R-Bound Empty Pocket State of G_α Is Conformationally Dynamic.* Our previous NMR results with light-activated rhodopsin (R*) and HPTRX−CDEF, a soluble mimic of R*, showed that stimulation of GDP−GTP exchange results in conformational changes in the switch II and carboxyl-terminal regions of G_α (*26*). Specifically, indole resonances assigned to Trp-207 in switch II are exchange broadened beyond detection, while amide resonances assigned to the carboxyl-terminal Phe-350 residue shift to an activated position in the GTPγS/Mg^{2+}-bound form of G_α generated upon interaction of the ^{15}N-ChiT reconstituted heterotrimer with R*. For HPTRX−CDEF, which forms a stable, stoichiometric complex with the GTPγS-exchanged heterotrimer, amide resonances assigned to Phe-350 also shift to the same activated position, while the $^{1}NH-^{15}N$ cross-peak of the Trp-207 indole resonates in a new downfield position relative to that observed previously for the GDP/Mg^{2+}-bound heterotrimer and GDP·AlF_4^-/Mg^{2+}-bound ChiT (*26*). The results presented here show that while both light-activated rhodopsin and HPTRX−CDEF proceed through an empty pocket state to yield their respective GTPγS-bound states of G_α, this reaction pathway intermediate is characterized by a severe exchange broadening of resonances that suggests the formation of a metastable, confomationally dynamic state of G_α (Figures 3 and 4). Moreover, the dynamic properties of this state do not appear to be a consequence of the loss of bound guanine nucleotide but rather to result primarily from R*-induced changes in the receptor-interacting regions of G_α as a GDP-depleted, Mg^{2+}-bound form of G_α generated in a manner independent of R* displays amide resonance chemical shifts similar to those observed in the GDP/Mg^{2+}-bound state of ^{15}N-ChiT (Figure 6B). It should be emphasized that since the HPTRX−CDEF·$G_{t\alpha\beta\gamma}$·GTPγS-exchanged complex displays a reasonably disperse and relatively sharp HSQC spectrum (Figure 4C), these findings suggest that the severe broadening of resonances in the R*-bound empty pocket heterotrimer state are not due to the relatively large size of these complexes (further discussed below) but rather to the intrinsic dynamic nature of G_α in this transient R*-bound state. Such dynamic character for G_α in the R*·$G_{\alpha\beta\gamma}$[empty] complex was not anticipated given the observed stabilization by R* by $G_{\alpha\beta\gamma}$ in both membranes (*27*) and detergent (Figure 2). However, recently reported electron spin resonance distance measurements using spin-labels incorporated at specific sites in $G_{\alpha i1}$ also suggest that G_α in the R*-bound empty pocket heterotrimer state may not adopt a single conformation but

rather exist as an ensemble distribution of conformations (*45*). While we cannot exclude the alternative possibility of transient GDP re-binding as a cause of the observed conformational exchange broadening of the G_α spectra in our experimental system at this time, we would note that the similarities in chemical shifts for resonances of corresponding residues in the HSQC spectra of GDP/Mg^{2+}-bound and GDP-depleted, Mg^{2+}-bound ChiT (Figure 6B) would make any exchange processes due to GDP re-binding likely unobservable.

While it is clear that the R*-bound empty pocket form of G_α represents an ensemble of two or more conformations which are exchanging at a rate that precludes observation of distinct species in our NMR spectra, the molecular mechanism(s) underlying this process remains to be discerned. In this context, it should be emphasized that a primary concern from the outset of these experiments has been the relatively large size of the R*−G-protein complexes and their suitability for NMR analysis. We would note that rhodopsin, and several other family A GPCRs, may form higher-order oligomers in the native membrane and in some detergents or lipid systems and that a dimeric structure may represent a functionally relevant form of the receptor (*22*, *46*−*49*). As the oligomeric status of rhodopsin in Cymal-5 has not yet been examined, the stoichiometry of rhodopsin relative to the G-protein heterotrimer in the R*−G-protein complexes examined under our NMR experimental conditions is currently unknown. While the minimum size for a rhodopsin−G-protein complex assuming a 1:1 stoichiometry is ~125 kDa (plus detergent molecules) and clearly represents a significant challenge for high-resolution NMR analysis, a second rhodopsin in the complex (i.e., a rhodopsin dimer bound to a single G-protein heterotrimer) would undoubtedly contribute to additional line broadening. Nonetheless, the observed line broadening observed in the presence of HPTRX−CDEF, which appears to form a 1:1 complex with the G-protein heterotrimer (*26*), suggests that the bound empty pocket state of the heterotrimer is conformationally dynamic regardless of the stoichiometry of components comprising the complex.

Comparisons of the NMR Results with Structures of Empty Pocket Monomeric GTPases in Complex with Cognate Guanine Nucleotide Exchange Factors (GEFs). Structural studies on elongation factor Tu−elongation factor Ts, Ras−Son of sevenless, and Rac1−T lymphoma invasion and metastasis factor 1 complexes have revealed that these GTPase−GEF complexes can be crystallized in a stable form in the absence of bound guanine nucleotide (an empty pocket state) (*50*−*53*). These GTPases utilize their cognate GEFs to catalyze the exchange of bound GDP for GTP and therefore proceed through a receptor-independent guanine nucleotide exchange mechanism. Interestingly, the overall structure of the empty pocket state of these GTPases, including the guanine nucleotide pocket region, is highly ordered, even more so than what has been observed for their guanine nucleotide-bound forms. Since our solution studies on GDP-depleted G_α generated in a manner independent of R* also show that the absence of bound guanine nucleotide has little impact on the overall conformation and dynamics of G_α, it would seem reasonable that G_α in the R*·$G_{\alpha\beta\gamma}$[empty] complex is not characterized by a similarly "ordered" conformation. In this respect, the apparent structural plasticity of G_α in the R*·$G_{\alpha\beta\gamma}$[empty] complex appears to be directly related to receptor interactions which are unique relative to those previously described for small GTPase−GEF complexes.

Functional Implications for the Mechanism of Guanine Nucleotide Exchange. We have developed a working model based on our previous NMR observations that also incorporates other fundamental results focused on elucidating changes in the structure of G_α that accompany heterotrimer formation and R* interactions (*26*). On the basis of the findings reported here, it would appear that the R*-induced perturbations in the conformation of G_α that facilitate GDP release and lead to the formation of the R*·$G_{\alpha\beta\gamma}$[empty complex] are of a nature that presently precludes a high-resolution understanding of the changes in the receptor-interacting and switch II regions of this intermediate R*-bound state of G_α. In particular, conformational changes following formation of the preactivated state of G_α attained upon association with $G_{\beta\gamma}$, which may poise the heterotrimer for R* interactions and GTP uptake (ref *25* and Figure 1), are no longer evident in the NMR spectra and therefore impede our ability to track functionally important changes in these and other regions of G_α in this R*-bound state(s) of the heterotrimer. Nonetheless, a conformationally dynamic R*-bound form of G_α may represent a functionally significant reaction pathway intermediate. For example, since G_α in this state has the capacity to bind both GDP and GTP (*27*), this may allow the progress of the reaction to be regulated by the available GTP:GDP ratio. As such, blending of this relatively early step of the phototransduction cascade with the biochemical pathways of guanine nucleotide metabolism (*54*) may provide an additional "checkpoint" for controlling the rate of R*-mediated signal propagation.

CONCLUSION

Our ability to generate and interrogate trapped R*-bound conformations of G_α by high-resolution NMR methods provides an opportunity to monitor conformational changes in G_α accompanying the complete cycle of R*−G-protein interactions. The observation of a metastable, dynamic conformation for G_α in both the light-activated rhodopsin and HPTRX−CDEF-bound $G_{\alpha\beta\gamma}$[empty] complexes, relative to the GDP-depleted, Mg^{2+}-bound state of G_α generated in a manner independent of R*, suggests that changes in the extreme amino and carboxyl termini of G_α that are thought to occur upon interaction with R*, rather than the absence of bound guanine nucleotide, are the predominant factors which govern G_α conformation and dynamics in the R*-bound empty pocket state. Thus far, we have trapped and analyzed two of the three R*-bound intermediates in the R*−G_t reaction pathway shown in Scheme 1: the R*·$G_{\alpha\beta\gamma}$-[empty] (step 3) and R*·$G_{\alpha\beta\gamma}$·GTP (step 4) complexes. It is anticipated that efforts focused on trapping and analyzing the conformation of G_α in the R*·$G_{\alpha\beta\gamma}$·GDP complex, in combination with the further assignment of chemical shifts for the various states of G_α, should allow the generation of models that describe in atomic detail the propagation of structural signals from the receptor binding interface of G_α to the guanine nucleotide-binding pocket.

ACKNOWLEDGMENT

We thank John Spudich, Kris Palczewski, and Dave Farrens for comments and suggestions during the course of these studies. We also thank John Putkey and Sudhir Paul for access to spectrofluorometer instrumentation.

REFERENCES

1. Coleman, D. E., Berghuis, A. M., Lee, E., Linder, M. E., Gilman, A. G., and Sprang, S. R. (1994) Structures of active conformations of Giα1 and the mechanism of GTP hydrolysis, *Science 269*, 1405−1412.
2. Lambright, D. G., Noel, J. P., Hamm, H. E., and Sigler, P. B. (1994) Structural determinants for activation of the α-subunit of a heterotrimeric G protein, *Nature 369*, 621−628.
3. Mixon, M. B., Lee, E., Coleman, D. E., Berghuis, A. M., Gilman, A. G., and Sprang, S. R. (1995) Tertiary and quaternary structural changes in Giα1 induced by GTP hydrolysis, *Science 270*, 954−960.
4. Noel, J. P., Hamm, H. E., and Sigler, P. B. (1993) The 2.2 Å crystal structure of transducin-α complexed with GTPγS, *Nature 366*, 654−663.
5. Sondek, J., Lambright, D. G., Noel, J. P., Hamm, H. E., and Sigler, P. B. (1994) GTPase mechanism of G proteins from the 1.7-Å crystal structure of transducin α-GDP-AlF_4^-, *Nature 372*, 276−279.
6. Sunahara, R. K., Tesmer, J. J., Gilman, A. G., and Sprang, S. R. (1997) Crystal structure of the adenylyl cyclase activator Gs, *Science 278*, 1943−1947.
7. Sondek, J., Bohm, A., Lambright, D. G., Hamm, H. E., and Sigler, P. B. (1996) Crystal structure of a G-protein βγ dimer at 2.1 Å resolution, *Nature 379*, 369−374.
8. Lambright, D. G., Sondek, J., Bohm, A., Skiba, N. P., Hamm, H. E., and Sigler, P. B. (1996) The 2.0 Å crystal structure of a heterotrimeric G protein, *Nature 379*, 311−319.
9. Wall, M. A., Coleman, D. E., Lee, E., Iniguez-Lluhi, J. A., Posner, B. A., Gilman, A. G., and Sprang, S. R. (1995) The structure of the G protein heterotrimer Gi $\alpha_1\beta_1\gamma_2$, *Cell 83*, 1047−1058.
10. Kreutz, B., Yau, D. M., Nance, M. R., Tanabe, S., Tesmer, J. J. G., and Kozasa, T. (2006) A new approach to producing functional Gα subunits yields the activated and deactivated structures of $G\alpha_{12/13}$ proteins, *Biochemistry 45*, 167−174.
11. Palczewski, K., Kumasaka, T., Hori, T., Behnke, C. A., Motoshima, H., Fox, B. A., Le Trong, I., Teller, D. C., Okada, T., Stenkamp, R. E., Yamamoto, M., and Miyano, M. (2000) Crystal structure of rhodopsin: A G-protein coupled receptor, *Science 289*, 739−745.
12. Teller, D. C., Okada, T., Behnke, C. A., Palczewski, K., and Stenkamp, R. E. (2001) Advances in determination of a high-resolution three-dimensional structure of rhodopsin, a model of G-protein-coupled receptors (GPCRs), *Biochemistry 40*, 7761−7772.
13. Okada, T., Fujiyoshi, Y., Silow, M., Navarro, J., Landau, E. M., and Schichida, Y. (2002) Functional role of internal water molecules in rhodopsin revealed by X-ray crystallography, *Proc. Natl. Acad. Sci. U.S.A. 99*, 5982−5987.
14. Okada, T., Sugihara, M., Bondar, A.-N., Elstner, M., Entel, P., and Buss, V. (2004) The retinal conformation and its environment in rhodopsin in light of a new 2.2 Å crystal structure, *J. Mol. Biol. 342*, 571−583.
15. Li, J., Edwards, P. C., Burghammer, M., Villa, C., and Schertler, G. F. X. (2004) Structure of bovine rhodopsin in a trigonal crystal form, *J. Mol. Biol. 343*, 1409−1438.
16. Ridge, K. D., Abdulaev, N. G., Sousa, M., and Palczewski, K. (2003) Phototransduction: Crystal clear, *Trends Biochem. Sci. 28*, 479−487.
17. Abdulaev, N. G., and Ridge, K. D. (2005) Structural and functional aspects of the mammalian rod cell photoreceptor rhodopsin, in *Handbook of Photosensory Receptors* (Briggs, W. R., and Spudich, J. L., Eds.) pp 77−92, Wiley-VCH Verlag GmbH & Co. KGaA, Weinheim, Germany.
18. Iri, T., Farfel, Z., and Bourne, H. R. (1998) G-Protein diseases furnish a model for the turn-on switch, *Nature 394*, 35−38.
19. Yeagle, P. L., and Albert, A. D. (2003) A conformational trigger for activation of a G protein by a G protein-coupled receptor, *Biochemistry 42*, 1365−1368.
20. Cherfils, J., and Chabre, M. (2003) Activation of G-protein Gα subunits by receptors through Gα-Gβ and Gα-Gγ interactions, *Trends Biochem. Sci. 28*, 13−17.
21. Herrmann, R., Heck, M., Henklein, P., Henklein, P., Kleuss, C., Hofmann, K. P., and Ernst, O. P. (2004) Sequence of interactions in receptor-G protein coupling, *J. Biol. Chem. 279*, 24283−24290.
22. Filipek, S., Krzysko, K. A., Fotiadis, D., Liang, Y., Saperstein, D. A., Engel, A., and Palczewski, K. (2004) A concept for G protein activation by G protein-coupled receptor dimers: The transducin/rhodopsin interface, *Photochem. Photobiol. Sci. 3*, 628−638.
23. Slusarz, R., and Ciarkowski, J. (2004) Interaction of class A G protein-coupled receptors with G proteins, *Acta Biochim. Pol. 51*, 129−136.
24. Abdulaev, N. G., Zhang, C., Dinh, A., Ngo, T., Bryan, P. N., Brabazon, D. M., Marino, J. P., and Ridge, K. D. (2005) Bacterial expression and one-step purification of an isotope-labeled heterotrimeric G-protein α-subunit, *J. Biomol. NMR 32*, 31−40.
25. Abdulaev, N. G., Ngo, T., Zhang, C., Dinh, A., Brabazon, D. M., Ridge, K. D., and Marino, J. P. (2005) Heterotrimeric G-protein α-subunit adopts a "preactivated" conformation when associated with βγ-subunits, *J. Biol. Chem. 280*, 38071−38080.
26. Ridge, K. D., Abdulaev, N. G., Zhang, C., Ngo, T., Brabazon, D. M., and Marino, J. P. (2006) Conformational changes associated with receptor-stimulated guanine nucleotide exchange in a heterotrimeric G-protein α-subunit: NMR analysis of GTPγS-bound states, *J. Biol. Chem. 281*, 7635−7648.
27. Bornancin, F., Pfister, C., and Chabre, M. (1989) The transitory complex between photoexcited rhodopsin and transducin. Reciprocal interaction between the retinal site in rhodopsin and the nucleotide site in transducin, *Eur. J. Biochem. 184*, 687−698.
28. Alves, I. D., Salgado, G. F., Salamon, Z., Brown, M. F., Tollin, G., and Hruby, V. J. (2005) Phosphatidylethanolamine enhances rhodopsin photoactivation and transducin binding in a solid supported lipid bilayer as determined using plasmon waveguide resonance spectroscopy, *Biophys. J. 88*, 198−210.
29. Kühn, H. (1980) Light- and GTP-regulated interaction of GTPase and other proteins with bovine photoreceptor membranes, *Nature 283*, 587−589.
30. Skiba, N. P., Bae, H., and Hamm, H. E. (1996) Mapping of effector binding sites of transducin α-subunit using $G_{\alpha t}/G_{\alpha i1}$ chimeras, *J. Biol. Chem. 271*, 413−424.
31. Ruan, B., Fisher, K. E., Alexander, P. A., Doroshko, V., and Bryan, P. N. (2004) Engineering subtilisin into a fluoride-triggered processing protease useful for one-step protein purification, *Biochemistry 43*, 14539−14546.
32. Abdulaev, N. G., Ngo, T., Chen, R., Lu, Z., and Ridge, K. D. (2000) Functionally discrete mimics of light-activated rhodopsin identified through expression of soluble cytoplasmic domains, *J. Biol. Chem. 275*, 39354−39363.
33. Fung, B. K. K., Hurley, J. B., and Stryer, L. (1981) Flow of information in the light-triggererd cyclic nucleotide cascade of vision, *Proc. Natl. Acad. Sci. U.S.A. 78*, 152−156.
34. Farrens, D. L., and Khorana, H. G. (1995) Structure and function in rhodopsin. Measurement of the rate of metarhodopsin II decay by fluorescence spectroscopy, *J. Biol. Chem. 270*, 5073−5076.
35. Guy, P. M., Koland, J. G., and Cerione, R. A. (1990) Rhodopsin-stimulated activation-deactivation cycle of transducin: Kinetics of the intrinsic fluorescence response of the α subunit, *Biochemistry 29*, 6954−6964.
36. Fahmy, K., and Sakmar, T. P. (1993) Regulation of the rhodopsin-transducin interaction by a highly conserved carboxylic acid group, *Biochemistry 32*, 7229−7236.
37. Faurobert, E., Otto-Bruc, A., Chardin, P., and Chabre, M. (1993) Tryptophan W207 in transducin Tα is the fluorescence sensor of the G protein activation switch and is involved in the effector binding, *EMBO J. 12*, 4191−4198.
38. Wessling-Resnick, M., and Johnson, G. L. (1987) Allosteric behavior in transducin activation mediated by rhodopsin. Initial rate analysis of guanine nucleotide exchange, *J. Biol. Chem. 262*, 3697−3705.
39. Ridge, K. D., Zhang, C., and Khorana, H. G. (1995) Mapping of the amino acids in the cytoplasmic loop connecting helices C and D in rhodopsin. Chemical reactivity in the dark state following single cytseine replacements, *Biochemistry 34*, 8804−8811.
40. Pereira, R., and Cerione, R. A. (2005) A switch 3 point mutation in the α subunit of transducin yields a unique dominant-negative inhibitor, *J. Biol. Chem. 280*, 35696−35703.

41. Grzesiek, S., and Bax, A. (1993) The importance of not saturating water in proton NMR. Application to selectivity enhancement and NOE measurements, *J. Am. Chem. Soc. 115*, 12593−12594.
42. Delaglio, F., Grzesiek, S., Vuister, G., Zhu, G., Pfeifer, J., and Bax, A. (1995) NMRPipe: A multidimensional spectral processing system based on UNIX pipes, *J. Biomol. NMR 6*, 277−293.
43. Mazzoni, M. R., and Hamm, H. E. (1996) Interaction of transducin with light-activated rhodopsin protects it from proteolytic digestion by trypsin, *J. Biol. Chem. 271*, 30034−30040.
44. Bubis, J., Ortiz, J. O., and Möller, C. (2001) Chemical modification of transducin with iodoacetic acid: Transducin-α carboxymethylated at Cys_{347} allows transducin binding to light-activated rhodopsin but prevents its release in the presence of GTP, *Arch. Biochem. Biophys. 395*, 146−157.
45. Oldham, W. M., Van Eps, N., Preininger, A. M., Hubbell, W. L., and Hamm, H. E. (2006) Mechanism of the receptor-catalyzed activation of heterotrimeric G proteins, *Nat. Struct. Mol. Biol. 13*, 772−777.
46. Liang, Y., Fotiadis, D., Filipek, S., Saperstein, D. A., Palczewski, K., and Engel, A. (2003) Organization of the G protein-coupled receptors rhodopsin and opsin in native membranes, *J. Biol. Chem. 278*, 21655−21662.
47. Medina, R., Perdomo, D., and Bubis, J. (2004) The hydrodynamic properties of dark- and light-activated states of n-dodecyl β-D-maltoside-solubilized bovine rhodopsin support the dimeric structure of both conformations, *J. Biol. Chem. 279*, 39565−39573.
48. Jastrzebska, B., Maeda, T., Zhu, L., Fotiadis, D., Filipek, S., Engel, A., Stenkamp, R. E., and Palczewski, K. (2004) Functional characterization of rhodopsin monomers and dimers in detergents, *J. Biol. Chem. 279*, 54663−54675.
49. Mansoor, S. E., Palczewski, K., and Farrens, D. L. (2006) Rhodopsin self-associates in asolectin liposomes, *Proc. Natl. Acad. Sci. U.S.A. 103*, 3060−3065.
50. Kawashima, T., Berthet-Colominas, C., Wulff, M., Cusack, S., and Leberman, R. (1996) The structure of the *Escherichia coli* EF-TuEF-Ts complex at 2.5 Å resolution, *Nature 379*, 511−518.
51. Wang, Y., Jiang, Y., Meyering-Voss, M., Sprinzl, M., and Sigler, P. B. (1997) Crystal structure of the EF-TuEF-Ts complex from *Thermus thermophilus*, *Nat. Struct. Biol. 4*, 650−656.
52. Boriack-Sjodin, P. A., Margarit, S. M., Bar-Sagi, D., and Kuriyan, J. (1998) The structural basis of the activation of Ras by Sos, *Nature 394*, 337−343.
53. Worthylake, D. K., Rossman, K. L., and Sondek, J. (2000) Crystal structure of Rac1 in complex with the guanine nucleotide exchange region of Tiam1, *Nature 408*, 682−688.
54. Abdulaev, N. G., Karaschuk, G. N., Ladner, J. E., Kakuev, D. L., Yakhyaev, A. V., Tordova, M., Gaidarov, I. O., Popov, V. I., Fujiwara, J. H., Chinchilla, D., Eisenstein, E., Gilliland, G. L., and Ridge, K. D. (1998) Nucleoside diphosphate kinase from bovine retina: Purification, subcellular localization, molecular cloning, and three-dimensional structure, *Biochemistry 37*, 13958−13967.
55. Medkova, M., Preininger, A. M., Yu, N. J., Hubbell, W. L., and Hamm, H. E. (2002) Conformational changes in the amino-terminal helix of the G protein α_{i1} following dissociation from Gβγ subunit and activation, *Biochemistry 41*, 9962−9972.

BI061088H